Supervised Classification and Estimation of Hydrometeors From C-Band Dual-Polarized Radars: A Bayesian Approach

Frank Silvio Marzano, *Senior Member, IEEE,* Daniele Scaranari, Mario Montopoli, and Gianfranco Vulpiani, *Member, IEEE*

***Abstract*—In this paper, a Bayesian statistical approach for supervised classification and estimation of hydrometeors, using a C-band polarimetric radar, is presented and discussed. The Bayesian Radar Algorithm for Hydrometeor Classification at C-band (BRAHCC) is supervised by a backscattering microphysical model, aimed at representing ten different hydrometeor classes in water, ice, and mixed phase. The expected error budget is evaluated by means of contingency tables on the basis of C-band radar noisy and attenuated synthetic data. Its accuracy is better than that obtained from a previously developed fuzzy logic C-band classification algorithm. As a second step of the overall retrieval algorithm, a multivariate regression is adopted to derive water content statistical estimators, exploiting simulated polarimetric radar data for each hydrometeor class. The BRAHCC methodology is then applied to a convective hail event, observed by two C-band dual-polarized radars in a network configuration. The hydrometeor classification along the line of sight, connecting the two C-band radars, is performed using the BRAHCC applied to path-attenuation-corrected data. Qualitative results are consistent with those derived from the fuzzy logic algorithm. Hydrometeor water content temporal evolution is tracked along the radar line of sight. Hail vertical occurrence is derived and compared with an empirical hail detection index applied along the radar connection line during the whole event.**

***Index Terms*—Bayesian inversion, hydrometeor classification and estimation, polarimetry, radar meteorology, rain clouds.**

I. Introduction

DUAL-POLARIZED weather radar systems can offer the capability to detect and identify different classes of hydrometeors within stratiform and convective storms [1]–[3], exploiting the sensitivity of polarimetric radar measurements to the microphysical properties of hydrometeors like composition, size, shape, and orientation [4]–[7]. Applications of hydrometeor classification may be various: detection of hailstorms, study of precipitating cloud microphysics, optimization of algorithms for precipitation rate retrieval, flight assistance, severe weather surveillance, and nowcasting.

Most hydrometeor classification techniques, either tuned for S- [6]–[9] or C-band data [10]–[13], have been so far developed on the basis of a fuzzy logic approach. Generally speaking, they show a high degree of flexibility and can be empirically adapted to experimental evidences by properly defining a class membership function (MBF) and an inference rule. Most classification algorithms share the idea that a polarimetric radar scattering simulator can provide a physically representative training data set for several classes of hydrometeors [6]–[9]. In this way, model-supervised fuzzy logic schemes have been so far designed for both S- and C-band data (e.g., [14]–[19]).

Indeed, the classification problem can also be approached by adopting different theoretical frameworks. The statistical decision theory, in the general form of the Bayesian formulation, may be an appealing detection and identification technique (e.g., [20]). With respect to a fuzzy logic approach, where the crucial step is the class MBF design, for a Bayesian approach, the critical issue is the modeling of the *a posteriori* class probability density function (pdf) (e.g., [21]). The latter is usually described by means of analytical functions, such as normal or log-normal pdfs, but any numerical histogram description can also be used. The Bayesian approach may have at least two advantages: 1) it can deal with a fully multidimensional domain of the observables, thus, including the relative variances and cross correlations when dealing with a second-order statistics and 2) a rigorous insertion of the *a priori* information within the detection procedure in terms of hydrometeor class occurrence, possibly related to environmental conditions and empirical knowledge.

Classification procedures aim to provide a class code which is not easy to compare with *in situ* data or other sources. A more natural product of an overall hydrometeor retrieval algorithm may be the estimation of the associated hydrometeor water content (e.g., [20]). In a way, within the signal theory framework, we are stating that, after the detection of the signal (hydrometeor class), it would be desirable to estimate some physical parameters (e.g., hydrometeor water content) [21]. The estimation of the hydrometeor water content is also very appealing since it

Manuscript received January 31, 2007; revised June 17, 2007. This work was supported in part by the Italian Ministry of University and Research, by Region Abruzzo, and by the Italian Department of Civil Protection.

F. S. Marzano is with the Department of Electronic Engineering, University of Rome "La Sapienza," 00184 Rome, Italy, and also with the Center of Excellence CETEMPS, University of L'Aquila, 67040 L'Aquila, Italy (e-mail: marzano@die.uniroma1.it).

D. Scaranari was with the Department of Electronic Engineering, University of Rome "La Sapienza," 00184 Rome, Italy and is currently with Sofiter System Engineering, 00195 Rome, Italy (e-mail: danielescaranari@tele2.it).

M. Montopoli is with the Department of Electrical and Information Engineering and also with the Center of Excellence CETEMPS, University of L'Aquila, 67040 L'Aquila, Italy (e-mail: mmontop@ing.univaq.it).

G. Vulpiani was with the Center of Excellence CETEMPS, University of L'Aquila, 67040 L'Aquila, Italy. He is now with the Dipartimento della Protezione Civile via Vitorchiano, 2 00189, Rome, Italy (e-mail: gianfranco.vulpiani@protezionecivile.it).

Color versions of one or more of the figures in this paper are available online at http://ieeexplore.ieee.org.

Digital Object Identifier 10.1109/TGRS.2007.906476

may allow direct comparison of radar products with numerical mesoscale cloud-model outputs, and to some extent, it may simplify the radar data assimilation within weather-forecast models [22]. Water content estimators are available in the literature, particularly at S-band, but no systematic analyses have been carried out exploiting polarimetric signatures at C-band [22].

In this paper, a new hydrometeor classification and estimation approach at C-band is proposed using a statistical Bayesian approach. The Bayesian Radar Algorithm for Hydrometeor Classification at C-band (BRAHCC) is supervised by a hydrometeor scattering model (briefly illustrated in Section II together with the estimation models of hydrometeor water contents). The Bayesian technique is described in Section III, where its classification accuracy is tested on synthetic radar data and compared with a fuzzy logic algorithm. Finally, in Section IV, the BRAHCC methodology is applied to a convective hail event observed by two C-band dual-polarized radars in network configuration. The results, along the connection line between the two radars, are analyzed, focusing on hydrometeor classification, water content retrieval, and hail detection.

II. Hydrometeor Radar Modeling and Water Contents

A hydrometeor ensemble backscattering model, based on the T-Matrix method, can be used in order to obtain hydrometeor polarimetric signatures and their relation with hydrometeor properties [23], [24]. The numerical model adopted here is microphysically based, as it uses a detailed description of hydrometeor shape, orientation, composition, and size distribution [25]. The polarimetric signature information, extracted from this numerical model, will be used to train the water content estimators and to supervise the classification scheme, as described in Sections II-B and III, respectively.

A. Polarimetric Observables and Microphysical Models

If D_e is the sphere-equivalent diameter and $N(D_e)$ represents the particle size distribution (PSD) for a specific hydrometeor, the copolar reflectivity factors $Z_{\rm hh,vv}$ are defined as

$$Z_{\rm hh,vv} = \frac{\lambda^4}{\pi^5 |K|^2} \int_0^\infty \sigma_{\rm hh,vv}(D_e) N(D_e) dD_e = \frac{\lambda^4 \langle \sigma_{\rm hh,vv} \rangle}{\pi^5 |K|^2} \tag{1}$$

where K is the dielectric complex factor [23]. In (1), $\sigma_{\rm hh,vv}$ is the copolar backscattering cross section at the horizontal and vertical polarizations, whereas the angle brackets stand for ensemble averaging over $N(D_e)$. The differential reflectivity $Z_{\rm dr}$ and specific differential phase $K_{\rm dp}$ are given by

$$Z_{\rm dr} = 10 \log_{10} \left(\frac{Z_{\rm hh}}{Z_{\rm vv}} \right) = 10 \log_{10} \left(\frac{\langle \sigma_{\rm hh} \rangle}{\langle \sigma_{\rm vv} \rangle} \right) \tag{2}$$

$$K_{\rm dp} = 10^{-3} \frac{180}{\pi} \lambda {\rm Re} \left\{ \int_0^\infty N(D_e) [f_{\rm hh}(r, D_e) - f_{\rm vv}(r, D_e)] dD_e \right\} \tag{3}$$

where $f_{\rm hh,vv}$ is the forward-scattering amplitude at the horizontal and vertical polarizations. Note that, in (2) and (3), $Z_{\rm dr}$ is expressed in decibels and $K_{\rm dp}$ in degrees per kilometer, whereas D_e and λ are expressed in millimeters so that $Z_{\rm hh,vv}$ are in megamillimeters per cubic meter. We limit our attention to these observables; the analysis of copolar correlation coefficient $\rho_{\rm hv}$ and linear-depolarization ratio $L_{\rm dr}$ are beyond our scopes.

For homogeneously distributed sphere-equivalent particles, the equivalent liquid water content, or simply water content (W), is defined as

$$W = 10^{-3} \frac{\pi}{6} \rho \int_0^\infty D_e^3 N(D_e) dD_e \tag{4}$$

where W is measured in grams per cubic meter, if the density ρ is expressed in grams per cubic centimeter. Both radar observables in (1)–(3) and the water content in (4) need $N(D_e)$ to be numerically simulated. A common choice for hydrometeor $N(D_e)$ is the normalized Gamma PSD, having the following general form [23]:

$$N(D_e) = N_w f(\mu) \left(\frac{D_e}{D_0} \right)^\mu e^{-(3.67+\mu)\frac{D_e}{D_0}} \tag{5}$$

where $f(\mu)$ is a function of the shape parameter μ only, D_0 (in millimeters) is the median-volume drop diameter, and N_w (in per millimeter per cubic meter) is the intercept parameter. For $\mu = 0$, (5) reduces to a typical inverse exponential PSD.

In order to perform a direct performance comparison with a previously developed Fuzzy logic Radar Algorithm for Hydrometeor Classification at C-band (FRAHCC), the same microphysical and dielectrical models, as described in [19] and [26], have been adopted here. The ten identified hydrometeor classes will be specified by an index c_i, with i ranging from zero to nine, as follows: large drops (LD, $i = 0$), light rain (LR, $i = 1$), medium rain (MR, $i = 2$), heavy rain (HR, $i = 3$), hail/rain mixture (H/R, $i = 4$), hail (H, $i = 5$), graupel/small hail (G/SH, $i = 6$), dry snow (DS, $i = 7$), wet snow (WS, $i = 8$), and ice crystals (IC, $i = 9$). The driving input parameters of the radar simulator are as follows: diameter range, random variation range of PSD parameters (N_w, D_0, and μ), model of relative dielectric constant, temperature range, axis-ratio model of ellipsoidal particle, and Gaussian pdf parameters of particle orientation [26].

B. Estimation of Hydrometeor Water Content

Since W is defined as the third-order moment of the PSD, it can be reasonably related to the copolar radar reflectivity factor $Z_{\rm hh}$ by a power-law relation, as for the rainfall rate R

$$W \cong a Z_{\rm hh}^b. \tag{6}$$

In order to justify a power-law estimation relation, we may deal with the Rayleigh scattering approximation, which is mainly valid at S-band [23]. If (5) holds, the liquid water

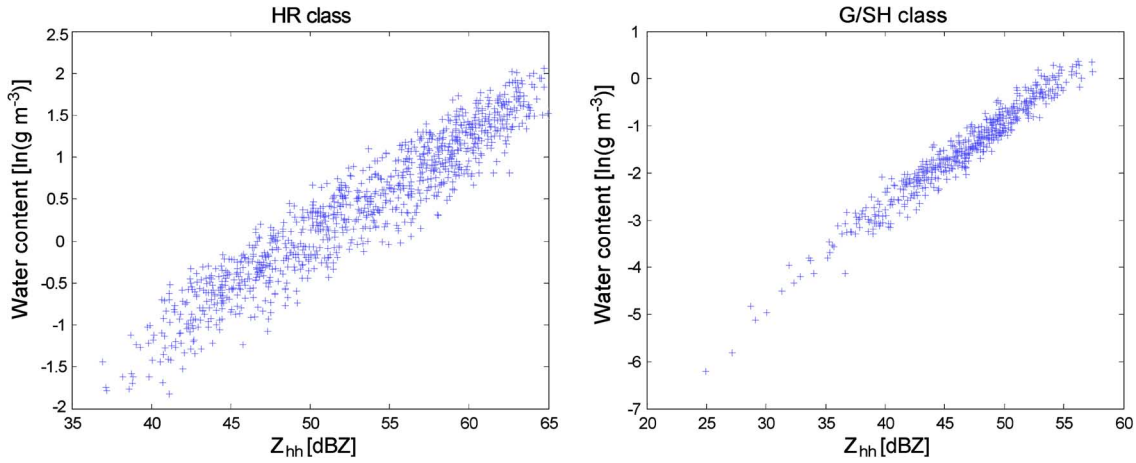

Fig. 1. Simulated copolar reflectivity $Z_{\rm hh}$ at C-band versus water content W for HR and G/SH class in logarithmic plane.

TABLE I
REGRESSION COEFFICIENTS TO ESTIMATE W BY (6) AND (8), WITH W IN GRAMS PER CUBIC METER, $Z_{\rm hh}$ IN MEGAMILLIMETERS PER CUBIC METER, AND $Z_{\rm dr}$ A DIMENSIONAL. RMSE IN GRAMS PER CUBIC METER AND FSE IN PERCENT ARE ALSO REPORTED

	Using Z_{hh}				*Using Z_{hh} and Z_{dr}*				
Class	*ln(a)*	*b*	*RMSE*	*FSE*	*ln(a')*	*b'*	*c'*	*RMSE*	*FSE*
LD	-9.3114	0.6404	0.0148	26.0	-8.9710	0.7205	-0.9937	0.0140	24.6
LR	-7.2143	0.7002	0.0380	38.9	-7.2265	0.7166	-0.6626	0.0368	37.7
MR	-6.8841	0.6154	0.1184	27.6	-7.3553	0.7066	-1.1477	0.1055	24.6
HR	-5.9015	0.5158	0.5960	30.0	-7.2863	0.6966	-1.0663	0.5137	25.8
H/R	-6.7157	0.5021	0.4213	26.7	-6.6150	0.4893	0.2241	0.4190	26.6
H	-11.1150	0.7620	0.1116	25.5					
G/SH	-10.1941	0.8105	0.0983	28.2					
DS	-8.9250	0.6950	0.0080	21.2					
WS	-6.2944	0.4545	0.0190	17.7					
IC	-8.9249	0.5882	0.0018	42.7					

content W is directly related to the DSD parameters D_0 and N_w [23] by the following relation:

$$W = \frac{\pi \cdot \rho}{10^3 \cdot (3.67)^4} \cdot D_0^4 \cdot N_w. \tag{7}$$

As shown in [36] and [37], for S-band radar data, either D_0 and N_w can be estimated by $Z_{\rm hh}$ and $Z_{\rm dr}$ measurements by means of empirical relations. The polarimetric power-law relationship with the inclusion of differential reflectivity $Z_{\rm dr}$ within the observable set may theoretically be justified, since $Z_{\rm dr}$ is strongly related to the median-volume diameter D_0 through the particle axis-ratio. It is then straightforward to pursue a polarimetric power-law relationship between $Z_{\rm hh}$, $Z_{\rm dr}$, and W of the form

$$W \cong a' Z_{\rm hh}^{b'} Z_{\rm dr}^{c'} \tag{8}$$

where a', b', and c' are the proper regression coefficients. On the basis of previous considerations, the statistical power-law models, as expressed by (6) and (8), can be supposed valid at C-band, as well as for all ten selected hydrometeor classes. An example of the relation between simulated $Z_{\rm hh}$ and W for the HR and G/SH class is shown in Fig. 1 in a logarithmic plane. In this plane, the linear relation between $Z_{\rm hh}$ and W is a fairly good choice, showing a correlation higher than 0.9.

In order to reproduce the radar measurement process, a zero-mean Gaussian noise with standard deviation of 1 dBZ and 0.3 dB has been added to simulated $Z_{\rm hh}$ and $Z_{\rm dr}$, respectively [25]. Sensitivity tests have been carried out for all hydrometeor classes using distinct data sets for training and testing. The analysis of relative performances has led to establish the optimal power-law relationship (e.g., see Fig. 1) to estimate W by means of a multiple-regression method, a special case of a Bayesian approach when a linearized model between parameters and measurement functions is assumed [27]. The obtained coefficients a and b for (6) and a', b', and c' for (8) are listed in Table I together with relative error budgets. The latter is expressed by means of the root mean square error (RMSE) and fractional standard error (FSE), defined as $\text{FSE} = 100 \cdot \text{RMSE}/\langle W \rangle$, where $\langle W \rangle$ is the ensemble average of W. The impact of $Z_{\rm dr}$ measurements is relevant only for water hydrometeor classes, whereas for ice hydrometeors (which have been supposed to be nearly spherical [26]), it does not give any particular improvement. For this reason, the model in (8) has been limited to water hydrometeor classes in Table I.

The power-law model might also be extended to $K_{\rm dp}$, whose estimate from radar measurements is not a trivial task (e.g., [23]). Moreover, for several classes such as LD, LR, H/R, H, DS, WS, and IC, the dynamic range of $K_{\rm dp}$ is below 2°/km. From our numerical tests, the improvement due to the use of

$K_{\rm dp}$ is expected particularly for MR, HR, and H/R hydrometeor classes, where FSE may even be lower than 15%.

III. Bayesian Classification of Hydrometeors

The Bayesian theory is quite a general inference methodology [28]. The statistical decision theory can be formulated resorting to the Bayes theory, introducing the concept of a risk defined as the expected value of the error cost function [21]. If the latter is assumed to be either a quadratic function or a uniform function, then the minimum mean square or maximum *a posteriori* probability (MAP) inference solutions, respectively, can be formulated. In this paper, the MAP inference rule, which is also called maximum-likelihood recognition in digital remote sensing [29], [30], is selected. The MAP algorithm is a computationally efficient and effective approach to the Bayesian classification in a supervised context, as in our case [20]. Theoretical, implementation, and verification issues are briefly described in the following.

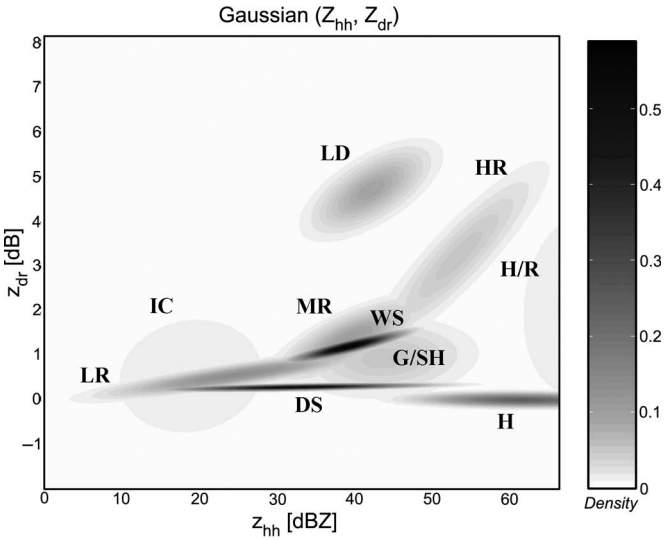

Fig. 2. Gaussian bivariate pdfs on the $(Z_{\rm hh}, Z_{\rm dr})$ plane, as derived from synthetic radar data simulations. Labels refer to hydrometeor classes (see text for details).

A. Theory and Implementation

A radar resolution volume can be characterized by a column vector $\mathbf{x}$ of size N_0, which includes both radar and possible meteorological observables, such as $Z_{\rm hh}$, $Z_{\rm dr}$, $K_{\rm dp}$, and local temperature T. Within the Bayesian theory, assigning correct hydrometeor classes to radar bins implies the knowledge of *a posteriori* (or posterior) conditional pdfs $p(c_i|\mathbf{x})$, where c_i is the unknown hydrometeor class with $i = 0, \ldots, 9$. The MAP decision rule is quite intuitive, as the hydrometeor class is provided by the index c_i that maximizes the conditional posterior pdfs

$$\mathbf{x} \in c_i \Leftrightarrow p\left(c_i|\mathbf{x}\right) > p\left(c_j|\mathbf{x}\right) \qquad \forall j \neq i. \tag{9}$$

The problem is that conditional posterior probabilities are usually unknown; but from the Bayes theorem, we have

$$p\left(c_i|\mathbf{x}\right) = \frac{p\left(c_i\right)p(\mathbf{x}|c_i)}{p(\mathbf{x})} \tag{10}$$

where $p(\mathbf{x}|c_i)$ is the conditional likelihood pdf, and $p(c_i)$ is the *a priori* (prior) pdf of hydrometeor class c_i. Using (9), (10) can be rewritten as follows:

$$\mathbf{x} \in c_i \Leftrightarrow p\left(\mathbf{x}|c_i\right)p\left(c_i\right) > p\left(\mathbf{x}|c_j\right)p\left(c_j\right) \qquad \forall j \neq i \tag{11}$$

where it is worth noting that $p(\mathbf{x})$ in (10) is constant with respect to c_i. In (11), both the likelihood and prior pdf must be expressed in order to evaluate the inference rule. This is one of the most critical issues of a Bayesian approach [28]. In a way, it resembles the choice of an MBF within fuzzy logic techniques, where a mix of prior knowledge and numerical results are combined to choose a proper (analytical) expression.

From a practical point of view, the likelihood pdf is usually assumed to be a multidimensional Gaussian pdf, as it largely simplifies the mathematical treatment of the Bayesian problem [29], [30]. This corresponds to assume that the polarimetric signatures of hydrometeor classes are hyperellipsoids in the multidimensional observation space. Indeed, the choice of a Gaussian likelihood pdf may also have a theoretical foundation under the conditions of steepness, smoothness, and concentration of $p(c_i|\mathbf{x})$ [28]. In other words, using an asymptotic analysis for a large sample, it can be shown that the Gaussian assumption holds if the following are attained: 1) inside a small neighborhood of the mean, the pdf is highly peaked and behaves like a "bell" function; and 2) the probability outside any neighborhood of the mean becomes negligible. The posterior and likelihood pdfs might be quantitatively analyzed by simply approximating the numerical histogram derived from the radar simulator, as described in Section II. However, the driving parameters are supposed to be uniformly varying without any specific knowledge of their experimental statistics [25]. This means that, at this stage, any pdf choice is quite arbitrary as it is, on the other hand, the choice of an MBF within the fuzzy logic theory.

Previous considerations suggest, to a first approximation, to assume that likelihood pdfs $p(\mathbf{x}|c_i)$ can be expressed in a multivariate Gaussian form

$$p(\mathbf{x}|c_i) = \frac{1}{\sqrt{(2\pi)^{N_0}}\sqrt{\det(\mathbf{C}_i)}} e^{-\left[\frac{1}{2}(\mathbf{x}-\mathbf{m}_i)^{\rm T}\mathbf{C}_i^{-1}(\mathbf{x}-\mathbf{m}_i)\right]} \tag{12}$$

where $\mathbf{m}_i$ is a column vector $(N_0 \times 1)$ containing mean values of the observables evaluated for the ith hydrometeor class, $\mathbf{C}_i$ is its autocovariance matrix $(N_0 \times N_0)$, and "T" and "-1" stand for matrix transpose and inverse, respectively. Mean vector and covariance matrix completely describe the multidimensional Gaussian pdf in (12), and they can be estimated by exploiting radar backscattering simulations. If we limit our attention to two radar observables $(N_0 = 2)$, i.e., $Z_{\rm hh}$ and $Z_{\rm dr}$, it is possible to create a tridimensional

TABLE II
TEMPERATURE RANGES AND CORRESPONDING SUPPRESSED HYDROMETEOR CLASSES. SUPPRESSION IS CARRIED OUT BY PREDEFINED SETS OF *A PRIORI* PROBABILITIES

Temperature range ΔT	$p(c_0)$ *LD*	$p(c_1)$ *LR*	$p(c_2)$ *MR*	$p(c_3)$ *HR*	$p(c_4)$ *H/R*	$p(c_5)$ *H*	$p(c_6)$ *G/SH*	$p(c_7)$ *DS*	$p(c_8)$ *WS*	$p(c_9)$ *IC*
<-52°C	0	0	0	0	0	0	0	0	0	1
-52°C ÷ -21°C	0	0	0	0	0	0	0.33	0.33	0	0.33
-21°C ÷ -11°C	0	0	0	0	0	0.25	0.25	0.25	0	0.25
-11°C ÷ -5°C	0	0	0	0	0.2	0.2	0.2	0.2	0	0.2
-5°C ÷ -3°C	0.2	0	0	0	0.2	0.2	0.2	0.2	0	0
-3°C ÷ 0°C	0.16	0	0	0	0.16	0.16	0.16	0.16	0.16	0
0°C ÷ +3°C	0.125	0.125	0.125	0.125	0.125	0.125	0.125	0	0.125	0
+3°C ÷ +10°C	0.14	0.14	0.14	0.14	0.14	0.14	0.14	0	0	0
+10°C ÷ +20°C	0.16	0.16	0.16	0.16	0.16	0.16	0	0	0	0
+20°C ÷ +30°C	0.2	0.2	0.2	0.2	0.2	0	0	0	0	0
>+30°C	0.25	0.25	0.25	0.25	0	0	0	0	0	0

view of the ten pdfs, as shown in Fig. 2. If projected onto the $Z_{\rm hh}$–$Z_{\rm dr}$ plane, Gaussian bivariate pdfs appear as a series of elliptical contours, concentric, and equiprobable [29]. Estimated mean vectors and covariance matrices are listed in the Appendix for both cases of three and four observables.

The *a priori* pdf $p(c_i)$ in (11) may be used to incorporate, in a rigorous framework, any *a priori* knowledge about the hydrometeor classes. Through this prior pdf, we can impose, for example, the existence of a class that is conditioned to radar measurements and environmental conditions. Due to lack of further information, we have simply exploited the temperature to suppress some hydrometeor classes that, we believe, cannot exist outside a given temperature range, following what was suggested in [8] and [26]. This means that the prior pdf can be approximated as

$$p(c_i) \cong p(c_i|T \in \Delta T) = P_i(\Delta T) \tag{13}$$

where ΔT is the temperature range, and P_i is the discrete probability of the ith class, depending on ΔT. Note that $\Sigma_i P_i(\Delta T) = 1$ holds. Temperature ranges of each hydrometeor class and their probabilities are shown in Table II. For a given ΔT, the probability of existing classes is uniformly redistributed as the first approximation holds. Temperature can be derived from local atmospheric radiosoundings, meteorological forecasts, or climatological models.

Taking the natural logarithm of $p(c_i|\mathbf{x})$ under the assumptions of (12) and (13) and inverting the sign, (9) becomes equivalent to minimizing a quadratic distance function $d(\mathbf{x}, c_i)$, which is also called metrics or discriminant function, with respect to c_i

$$d(\mathbf{x}, c_i) = \left\{ (\mathbf{x} - \mathbf{m}_i)^{\rm T} \mathbf{C}_i^{-1} (\mathbf{x} - \mathbf{m}_i) + \ln\left[\det(\mathbf{C}_i)\right] - 2\ln\left[p(c_i)\right] \right\}. \tag{14}$$

Thus, the MAP decision rule can finally be rewritten as

$$\mathbf{x} \in c_i \Leftrightarrow \begin{cases} d(\mathbf{x}, c_i) < d(\mathbf{x}, c_j) & \forall j \neq i \\ d(\mathbf{x}, c_i) < d_{\rm th}, \end{cases} \tag{15}$$

where $d_{\rm th}$ is a threshold. Since it is always possible to find a minimum for the distance function d, which is given by (14), a constraint has to be imposed to obtain physically meaningful results. This condition, which can be either applied to pdf or to distance functions, is often called decision thresholding in maximum-likelihood classification [29]. In our case, if the minimum distance $d(\mathbf{x}, c_i)$ is larger than a decision threshold $d_{\rm th}$, the corresponding radar bin is labeled as "not classified" (NC). The decision threshold is usually determined in an empirical way.

B. Test on Synthetic Data and Comparison With Fuzzy Logic

In order to evaluate the expected hydrometeor classification accuracy, we have generated a training and test data set consisting of 2000 independent simulations of $Z_{\rm hh}$, $Z_{\rm dr}$, $K_{\rm dp}$, and T for each hydrometeor class [26]. After some numerical tests, the decision threshold $d_{\rm th}$ to apply (17) has been set equal to 40 for the three observable configuration (i.e., $Z_{\rm hh}$, $Z_{\rm dr}$, and T) and 60 if $K_{\rm dp}$ is also considered.

As in [26], contingency tables have been then used to evaluate the classification accuracy on synthetic radar data [29]. It may be useful to recall some indexes: the producer accuracy (PA) along each column, the user accuracy (UA) along each row and its average $\rm UA_{av}$, and the overall accuracy (OA) which stands for the percentage ratio between the correctly classified samples over the total ones. The percentage of the NC samples and its average $(\rm NC_{av})$ over the ten hydrometeor classes are effective indicators of robustness to noise. Classification results, using only $Z_{\rm hh}$, $Z_{\rm dr}$, and T, are presented in Table III. G/SH and DS classes show the smallest UA

TABLE III
CONTINGENCY TABLE OBTAINED USING C-BAND BAYESIAN CLASSIFICATION ALGORITHM (BRAHCC) APPLIED TO C-BAND $Z_{\rm hh}$ AND $Z_{\rm dr}$ SIMULATED NOISY DATA TOGETHER WITH TEMPERATURE T

2 radar obs.		SIMULATION										C-band
		LD	LR	MR	HR	H/R	H	G/SH	DS	WS	IC	UA
CLASSIFICATION	LD	95%	0%	0%	2%	0%	0%	0%	0%	0%	0%	98%
	LR	0%	72%	10%	1%	0%	0%	2%	0%	3%	0%	83%
	MR	0%	22%	79%	11%	0%	0%	3%	0%	11%	0%	63%
	HR	2%	0%	6%	84%	1%	0%	0%	0%	0%	0%	91%
	H/R	0%	0%	0%	2%	81%	10%	0%	0%	0%	0%	87%
	H	0%	0%	0%	0%	17%	88%	3%	0%	0%	0%	81%
	G/SH	0%	4%	3%	0%	1%	2%	73%	25%	26%	0%	54%
	DS	3%	0%	0%	0%	0%	0%	17%	61%	5%	29%	53%
	WS	0%	1%	3%	0%	0%	0%	2%	0%	55%	0%	89%
	IC	0%	0%	0%	0%	0%	0%	0%	13%	0%	71%	84%
	PA	95%	72%	79%	84%	81%	88%	73%	61%	55%	71%	OA=76%
	NC	0%	0%	0%	0%	0%	0%	0%	0%	0%	0%	NC_{av}=0%

TABLE IV
SAME AS IN TABLE II BUT APPLIED TO C-BAND $Z_{\rm hh}$, $Z_{\rm dr}$, AND $K_{\rm dp}$ SIMULATED NOISY DATA

3 radar obs.		SIMULATION										C-band
		LD	LR	MR	HR	H/R	H	G/SH	DS	WS	IC	UA
CLASSIFICATION	LD	95%	0%	0%	0%	0%	0%	0%	0%	0%	0%	100%
	LR	0%	70%	7%	1%	1%	0%	1%	0%	1%	0%	87%
	MR	0%	24%	84%	10%	0%	0%	2%	0%	9%	0%	65%
	HR	2%	0%	4%	86%	0%	0%	0%	0%	0%	0%	94%
	H/R	0%	0%	0%	2%	89%	6%	0%	0%	0%	0%	92%
	H	0%	1%	0%	0%	9%	92%	3%	0%	0%	0%	88%
	G/SH	0%	4%	3%	0%	1%	1%	79%	38%	34%	1%	49%
	DS	3%	0%	0%	0%	0%	1%	13%	49%	3%	29%	50%
	WS	0%	1%	3%	0%	0%	0%	2%	0%	53%	0%	89%
	IC	0%	0%	0%	0%	0%	0%	0%	13%	0%	71%	84%
	PA	95%	70%	84%	86%	89%	92%	79%	49%	53%	71%	OA=77%
	NC	0%	0%	0%	0%	0%	0%	0%	0%	0%	0%	NC_{av}=0%

due to their reciprocal confusion. H/R, as expected, partially overlaps with H, whereas MR is slightly superimposed to LR and HR. Classification results, when $K_{\rm dp}$ is also considered as input, are shown in Table IV. Both OA and UA slightly increase due to the improvements of the PA and the UA for liquid and mixed-phase hydrometeor classification at the expense of DS and WS. Global accuracies in terms of OA, $\rm UA_{av}$, and $\rm NC_{av}$ are synthetically shown in Table V in order to perform a systematic comparison with a C-band fuzzy logic technique, which was previously developed and named FRAHCC [19], [26]. The clear improvement for OA and $\rm NC_{av}$ when using BRAHCC is remarkable, particularly in the case of three observables. The average number $\rm NC_{av}$ of the NC samples of BRAHCC is much less than that shown by FRAHCC. It is worth noting that, after a numerical

TABLE V
SUMMARY OF GLOBAL CLASSIFICATION PERFORMANCES, IN TERMS OF OA, $\rm UA_{av}$, AND $\rm NC_{av}$, PROVIDED BY FRAHCC AND BRAHCC FOR THREE AND FOUR OBSERVABLES

	OA (%)	UA_{av}*(%)*	NC_{av}*(%)*
BRAHCC (3 obs.)	76	78	0
FRAHCC (3 obs.)	68	78	12
BRAHCC (4 obs.)	77	80	0
FRAHCC (4 obs.)	75	79	3

TABLE VI
BRAHCC CLASSIFICATION PERFORMANCES AS IN TABLE VI, WHEN PROGRESSIVE NEGATIVE BIASES, DUE TO HYPOTHETICAL RAIN AND GRAUPEL SLABS, ARE APPLIED FOR THE CASE OF THREE AND FOUR OBSERVABLES

			3 observables			*4 observables*		
	Bias Z_{hh} (dBZ)	***Bias Z_{dr} (dB)***	***UA %***	***OA %***	***NC_{av} %***	***UA %***	***OA %***	***NC_{av} %***
Rain slab	-0.5	-0.15	78	75	0	80	77	0
	-1.5	-0.45	73	68	1	76	72	0
	-2.5	-0.75	65	59	3	68	63	1
	-3.5	-1.05	54	49	5	57	54	2
	-4.5	-1.35	43	43	7	48	47	4
Graupel slab	-0.5	-0.09	78	75	0	80	77	0
	-1.5	-0.27	77	74	0	79	76	0
	-2.5	-0.45	73	69	1	76	72	0
	-3.5	-0.63	68	63	2	71	67	1
	-4.5	-0.81	64	58	3	66	61	1

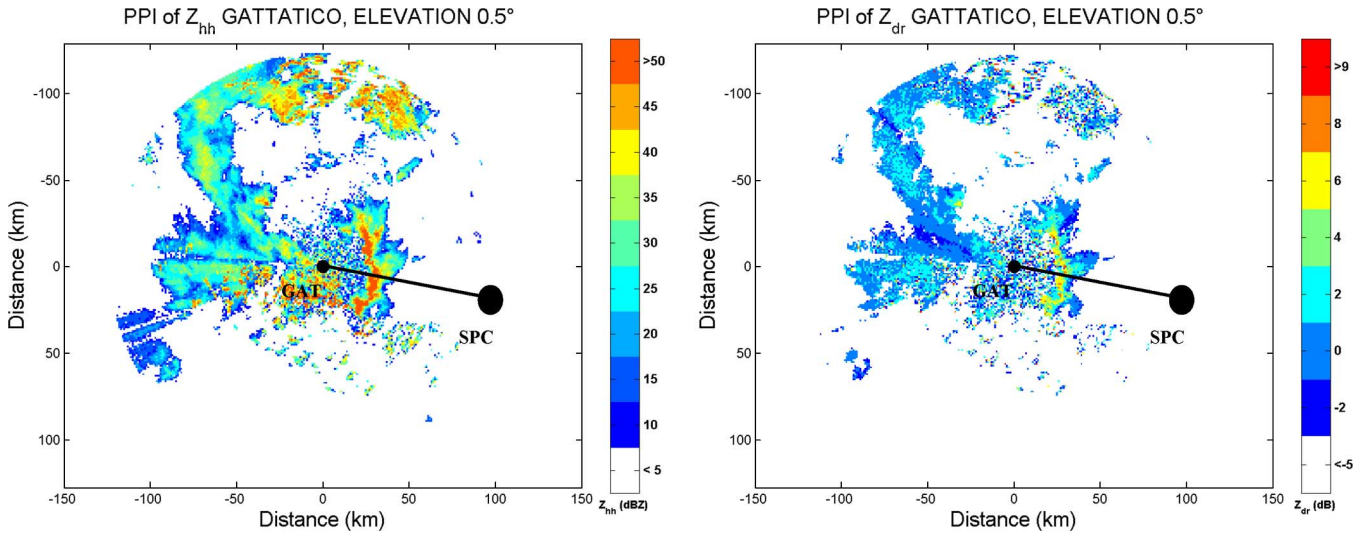

Fig. 3. PPIs of (left panel) copolar horizontal reflectivity $Z_{\rm hh}$ and (right panel) of differential reflectivity $Z_{\rm dr}$, measured at 16:34 GMT by the Gattatico radar. The black line indicates the line of sight between the two radar sites, depicted as black circles.

optimization, the current implementation of BRAHCC both with three or four observables, detects DS by means of $Z_{\rm hh}$ and T only, while LR is classified by $Z_{\rm hh}$, $Z_{\rm dr}$, and T (see the Appendix).

Following the same procedure outlined in [26], we have schematically tested the impact of path integrated attenuation (PIA) on BRAHCC classification performances. The basic idea is to suppose each random simulation as hypothetically measured after path attenuation due to either a rain or graupel slab. The noisy simulated values of $Z_{\rm hh}$ and $Z_{\rm dr}$ (derived from $Z_{\rm hh}$ for self-consistency) have been varied by an increasing negative bias, due to PIA, between -0.5 and -5 dB. Overall results, in terms of UA, OA, and $\rm NC_{av}$, are reported in Table VI. In the presence of PIA, as expected, global accuracies are obviously worse. In case of two radar observables, OA can be less than 50% if rain PIA is higher than 3.5 dB. The impact of graupel integrated attenuation is less pronounced than that due to a rain slab. If compared with the corresponding table of FRAHCC-classification results [26], the $\rm NC_{av}$ bins given by BRAHCC are always lower with respect to FRAHCC. If four observables are used, $\rm NC_{av}$ is never greater than 4%, while FRAHCC provides $\rm NC_{av}$ values up to 15% or over.

IV. APPLICATION TO A CASE STUDY

In this section, we will briefly describe the application of the overall retrieval BRAHCC procedure to a selected rain event. Two retrieval steps are in cascade: 1) first, for each radar bin, a hydrometeor classification is performed using (14) and (15); and 2) second, for the discriminated class, the water content is estimated through (8) and (10). If operating at C-band, path attenuation may play a significant impact and should be corrected for.

Available radar data refer to a convective episode that occurred in the region between two dual-polarized C-band systems, both located in the Po valley and about 90 km far apart: the S. Pietro Capofiume (SPC) and the Gattatico (GAT) radars, placed at an altitude of 11 and 34 m above the sea level, respectively. These radars can, unfortunately, only provide measurements of copolar and differential reflectivities. Fig. 3 shows the plan position indicator (PPI) maps of $Z_{\rm hh}$ and $Z_{\rm dr}$, respectively, measured at 16:34 GMT from the GAT radar at the lowest elevation angle of 0.5° (for more details about the radar system network and the hailstorm event description, in terms of vertical sections, refer to [13], [18], [19], and [26]).

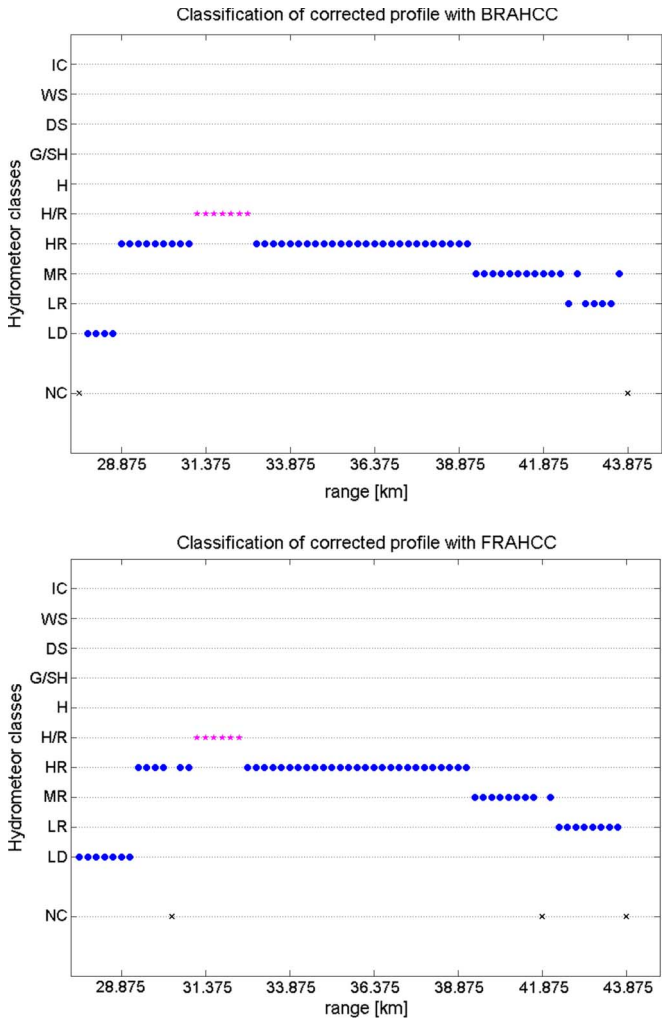

Fig. 4. (Top panel) BRAHCC algorithm with constrained inversion path attenuation correction. (Bottom panel) FRAHCC algorithm with constrained inversion path attenuation correction.

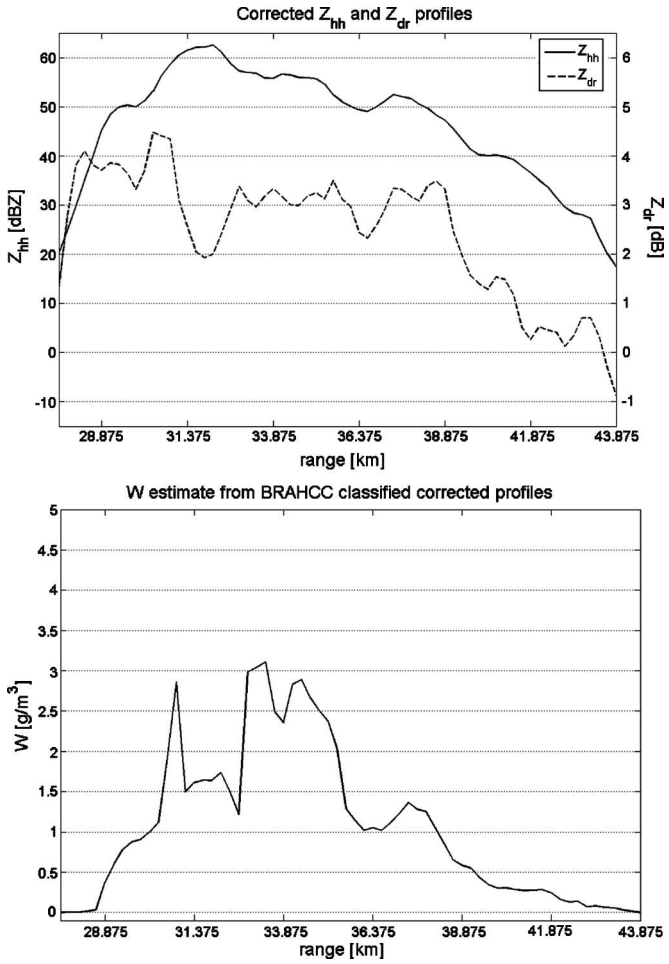

Fig. 5. (Bottom panel) Water content estimate, applied to the data in Fig. 4, using the BRAHCC algorithm, together with constrained inversion path attenuation correction. (Top panel) Corrected horizontal reflectivity and differential reflectivity are shown for comparison.

A. *Hydrometeor Classification and Water Content Estimate*

The two C-band radar systems, considered here, were unfortunately unable to measure the range profile of the differential phase shift $\Phi_{\rm dp}$. The latter is essential not only to extract $K_{\rm dp}$ but also to provide an estimate of the total path attenuation needed to estimate the specific attenuation along the storm core (e.g., [25] and [31]). In order to correct for PIA, we can exploit the network radar observation of this hailstorm by using either a radar maximum-reflectivity composite or a constrained-inversion algorithm, as illustrated in [26]. Once the range profiles of $Z_{\rm hh}$ and $Z_{\rm dr}$ have been corrected, any hydrometeor classification algorithm at C-band can be applied, using the temperature data from a close radiosounding station at 12:00 GMT.

Fig. 4 illustrates the results obtained using both BRAHCC and FRAHCC applied to the attenuation-corrected profile along the same radar line GAT–SPC. This comparison may also represent a qualitative check of the consistency between the two approaches. At the radar's lowest elevation angle, we are observing the convective core of the storm. This feature emerges from the predominance of HR with some LD on the storm left edge and H/R embedded within the storm core. The MR and LR classes characterize the right edge of the storm. The performances of BRAHCC and FRAHCC in terms of hydrometeor class detection are fairly comparable, as expected from the numerical analyses reported in Section III. FRAHCC technique tends to identify more LD than BRAHCC, whereas the H/R core and HR band are detected at the same range.

Fig. 5 shows the range profile of the water content estimate derived from (8), in case of rain and H/R, and from (6), in case of G/SH. The range profiles of the corrected $Z_{\rm hh}$ and $Z_{\rm dr}$ are also shown for comparison. As physically reasonable, the water content within the storm core around 30 km is larger and highly variable. Deep decreasing of W is noted before 32-km range associated to a decrease of $Z_{\rm dr}$ and to the presence of H/R. As clearly shown in Fig. 1, for a given reflectivity, the estimated water content is strongly dependent on the classified hydrometer class. Using the previous results, the time evolution of the water content estimates from about 15:30 to 21:50 GMT is worth analyzing. This picture, as shown in Fig. 6, can give an appealing overview of the potential of combining classification and estimation, using radar measurements. This range–time diagram clearly shows the movement toward east of the storm with a deintensification after 19:00 GMT.

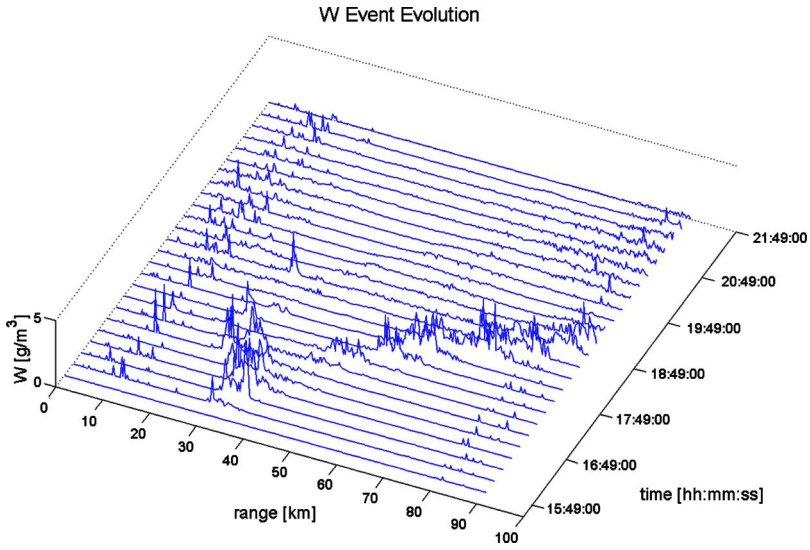

Fig. 6. Range–time diagram of the water content estimates after BRAHCC classification during the event along the radar connection line, corrected with constrained inversion technique, from 15:34 to 21:49 GMT. GAT radar is located on the west side at range $r = 0$.

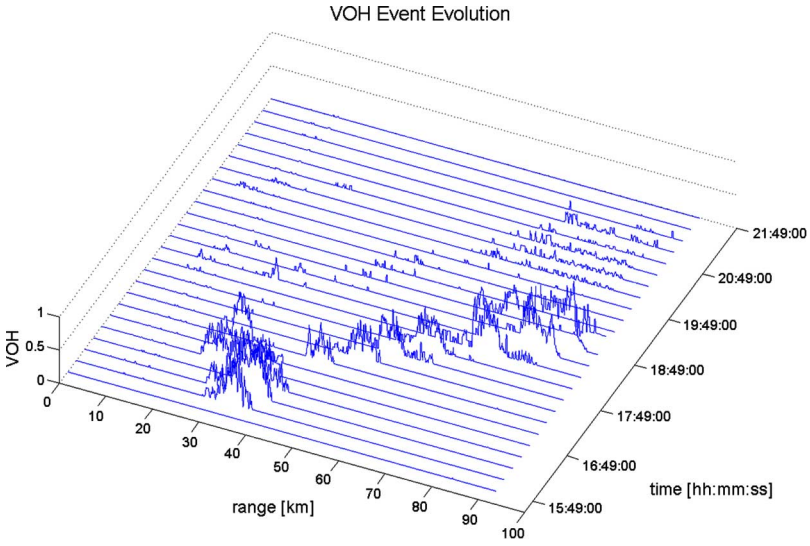

Fig. 7. Same as in Fig. 6 but for the VOH index, as defined by (16).

B. Hail Detection Analysis

The evolution of hail can be appreciated by exploiting the hydrometeor classification results [32]. After performing a Cartesian projection of the vertical section originally expressed in polar coordinates, each vertical profile is analyzed, and the occurrence $N_{c_i}(r,t)$ of each class c_i is counted for each discrete range r and time t. In case of hail (H and H/R), this number is named as $N_{\mathrm{H}}(r,t)$. The vertical occurrence of hail (VOH) index is then defined as

$$\mathrm{VOH}(r,t) = \frac{N_{\mathrm{H}}(r,t)}{\mathrm{Max}\left[N_{\mathrm{H}}(r,t)\right]} \tag{16}$$

where Max is the maximum searched within all available distances and time steps. This normalization is, indeed, arbitrary as it might be referred to a single event in a given area but, in general, taken from a proper database-library collecting rain events of different typology, season, and cyclogenesis. In this example, for simplicity, we have considered the maximum within the considered event so that VOH is normalized to one. The range–time diagram of VOH is shown in Fig. 7. The storm hail core is clearly detected, and its movement follows the displacement of the total water content near the ground, as plotted in Fig. 6.

The previous figure can be conveniently compared with an empirical index, which is the probability of hail (POH). The POH is estimated from the radar reflectivity data following the method of Waldvogel *et al.* [33]. It is based on the difference ΔH (in kilometers) between the height of the freezing level and the maximum height at which a reflectivity of 45 dBZ is observed (i.e., echotop 45 dBZ). The POH is calculated as follows [34]:

$$\mathrm{POH}(r,t) = 0.319 + 0.133 \cdot \Delta H(r,t). \tag{17}$$

This expression has been obtained from a verification study carried out in the summer of 2000 in The Netherlands [34].

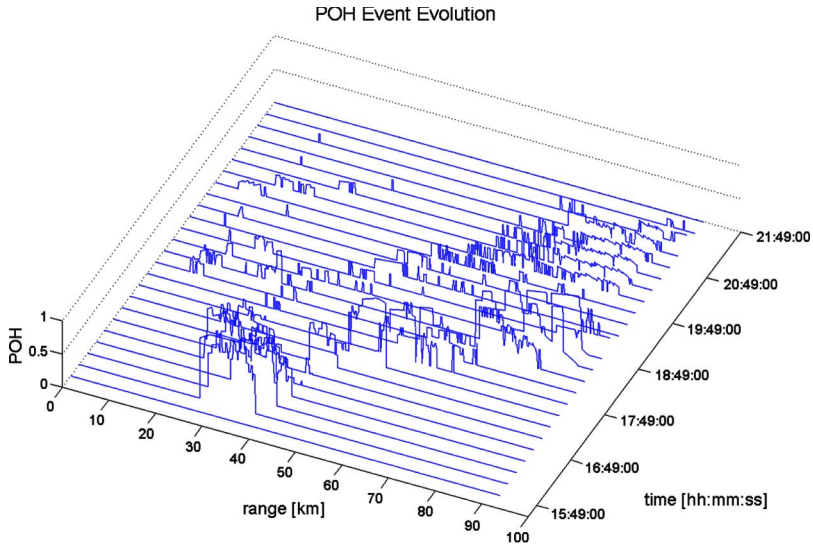

Fig. 8. Same as in Fig. 7 but for the POH index, as defined by (17) [33].

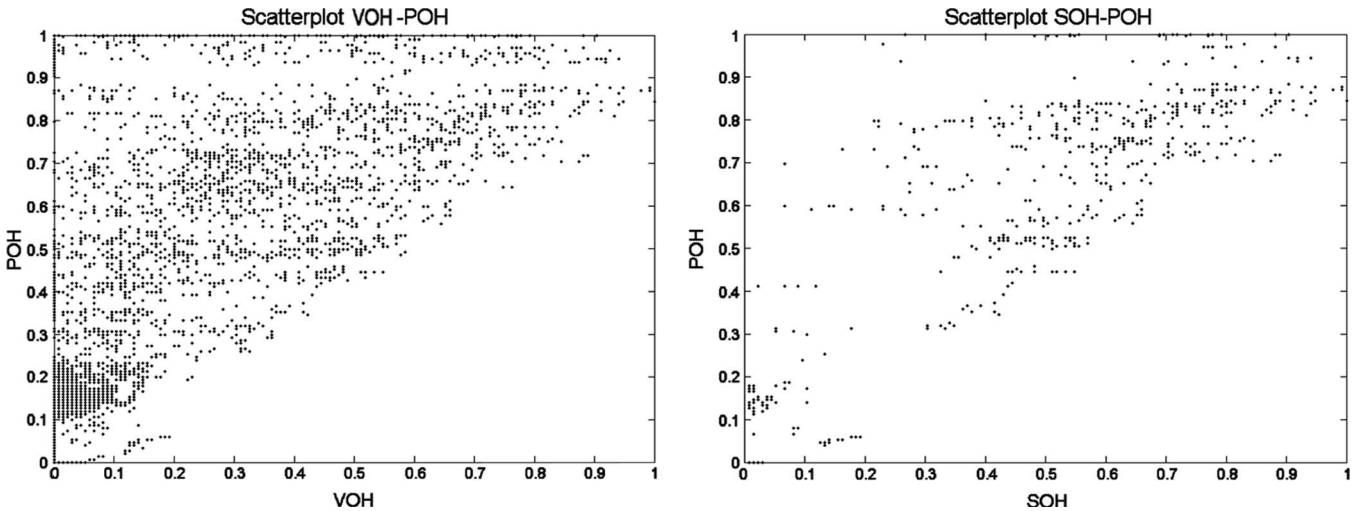

Fig. 9. Scatter plot of POH index versus the VOH and the SOH, defined as VOH when hail is detected at the lowest radar bin and zero, otherwise (see text for details).

The method combines an indicator for the presence of a substantial updraft (i.e., the height of the strong reflectivity core at 45 dBZ) with that for a large amount of supercooled water and/or ice (i.e., the reflectivity core above the freezing level). The probability of the presence of hail increases as the height of the reflectivity core increases. The POH method is also currently being used in the NEXRAD hail detection algorithm [35]. Fig. 8 shows the range–time diagram of POH, as shown in Fig. 6. The consistency between the POH and the VOH evolution is worth noticing. The difference between the intensities of the two indexes, particularly for time after 19:00 GMT, may be due not only to the climatic normalization and different empirical tuning but also to the intrinsic differences between the two indexes. Occurrences of hail in the vertical column are not necessarily related to the POH at the surface.

Using a correlation diagram for the whole event as in Fig. 9, we can note that a large POH may be associated to any value of VOH, whereas a small POH is related to a small VOH. This behavior may be explained since a large hail at the surface, as estimated by the POH, may be associated to small or large values of VOH. To prove this conjecture, from BRAHCC hydrometeor maps, we have evaluated the surface occurrence of hail (SOH), defined as the value of VOH when hail is detected at the lowest radar bin, and zero for all other occurrences

$$\mathrm{SOH}(r,t) = \mathrm{Surf}(r,t)\mathrm{VOH}(r,t) \tag{18}$$

where $\mathrm{Surf}(r,t)$ is a binary mask equal to one if hail is detected at the lowest radar bin and to zero, otherwise. As expected, the correlation between POH and SOH is much higher than that between POH and VOH, as the definitions of these two indexes POH and SOH are more homogeneous with respect to the hail detection.

V. Conclusion

A hydrometeor classification method, which is based on the Bayesian statistical approach and supervised by a backscattering microphysical model, has been introduced and discussed

for C-band polarimetric radar data applications. The method, named BRAHCC, is trained by synthetic data derived from fully polarimetric simulations for ten different hydrometeor classes. The expected error budget has been evaluated by means of contingency tables on the basis of C-band radar synthetic data. Sensitivity of BRAHCC to path-attenuation bias has been evaluated. After the classification step, a statistical multivariate regressive algorithm has been proposed to estimate the water content from C-band polarimetric radar data for each hydrometeor class. The radar estimation of water contents is appealing not only per se but also because it would provide a product that is easily comparable with mesoscale cloud-resolving models. Finally, the water content retrieval would open the opportunity for its direct assimilation into meteorological forecast numerical models [22].

This numerical analysis has shown that the Bayesian approach can provide a classification accuracy which is usually better than that, or at least comparable to, obtainable from other established approaches, based on fuzzy logic techniques at C-band. It is worth stressing that the Bayesian approach to classification presents some interesting features: 1) The *a priori* information can be introduced within the algorithm by modeling the prior pdf; 2) the algorithm can be easily updated if improved microphysical models are set up and new frequency bands are of interest, since the likelihood Gaussian pdf is simply defined by mean vector and covariance matrices of class ensemble; 3) it does not require any factorization assumption of the multidimensional observation space, as usually necessary when designing MBFs within fuzzy logic approaches; and 4) if needed, the Gaussian assumption for the likelihood pdf may be substituted with other analytical pdfs or even numerical histograms when experimental evidences emerge.

The BRAHCC methodology has been then applied to a convective hail event within a region located between two C-band dual-polarized radars. The radar network configuration has been exploited to correct for C-band path attenuation [26]. The hydrometeor classification along the line of sight, connecting the two C-band radars, has been performed using BRAHCC applied to path-attenuation corrected data. The results have been compared with FRAHCC, confirming a consistency between the Bayesian and fuzzy logic approaches. Products have been shown for rain, graupel, and hail along the line of sight during the event temporal evolution. As a further analysis, hail occurrence has also been estimated and compared with an empirical hail detection algorithm.

A critical point of this paper, as of many others on hydrometeor classification, is the difficulty to perform a robust validation of the obtained results. We have tackled this problem by resorting both to synthetic radar and microphysical data and to a visual inspection of the product physical consistency. As a matter of fact, it is not easy to experimentally assess hydrometeor classification accuracy within fine radar resolved volumes of a few hundred meters. On one hand, airborne sampling may not be spatially representative, and on the other hand, it may be difficult to colocate the measurements in space and time. Moreover, we are usually able to estimate from radars the most probable class, avoiding the possible existence of several hydrometeor classes within the same resolution volume. Anyway, the capability to convert the hydrometeor class product into water content estimates may facilitate these comparisons with *in situ* data.

APPENDIX
BAYESIAN CLASSIFICATION ALGORITHMS

Estimates of the mean vectors and covariance matrices for the set of ten selected hydrometeor classes are reported to practically apply BRAHCC. Such data are necessary in order to calculate distance function in (14). The following notation is adopted: A superscript indicates the number of radar observables (i.e., "2 obs," "3 obs") used in the current implementation, whereas a subscript indicates the considered hydrometeor class.

Two-Observable Radar Measurements

In this case, we are supposing to have, at disposal, a column vector of measurements $\mathbf{x} = [T, Z_{\rm hh}, Z_{\rm dr}]^{\rm T}$, where T is in degree Celsius, $Z_{\rm hh}$ is in decibel of Z, and $Z_{\rm dr}$ is in decibels

$$\mathbf{m}_{LD}^{\rm 2obs} = \begin{bmatrix} 15.106 \\ 42.946 \\ 4.717 \end{bmatrix} \quad \mathbf{C}_{LD}^{\rm 2obs} = \begin{bmatrix} 133.86 & 2.276 & 0.245 \\ 2.276 & 61.947 & 4.081 \\ 0.245 & 4.081 & 0.371 \end{bmatrix}$$

$$\mathbf{m}_{LR}^{\rm 2obs} = \begin{bmatrix} 20.106 \\ 25.743 \\ 0.548 \end{bmatrix} \quad \mathbf{C}_{LR}^{\rm 2obs} = \begin{bmatrix} 133.86 & -2.226 & -0.112 \\ -2.226 & 78.725 & 2.047 \\ -0.112 & 2.047 & 0.071 \end{bmatrix}$$

$$\mathbf{m}_{MR}^{\rm 2obs} = \begin{bmatrix} 20.106 \\ 39.95 \\ 1.375 \end{bmatrix} \quad \mathbf{C}_{MR}^{\rm 2obs} = \begin{bmatrix} 133.86 & -1.783 & -0.502 \\ -1.783 & 14.216 & 0.887 \\ -0.502 & 0.887 & 0.148 \end{bmatrix}$$

$$\mathbf{m}_{HR}^{\rm 2obs} = \begin{bmatrix} 20.106 \\ 54.097 \\ 3.547 \end{bmatrix} \quad \mathbf{C}_{HR}^{\rm 2obs} = \begin{bmatrix} 133.86 & -0.275 & 2.154 \\ -0.275 & 33.607 & 5.642 \\ 2.154 & 5.642 & 1.256 \end{bmatrix}$$

$$\mathbf{m}_{H/R}^{\rm 2obs} = \begin{bmatrix} 10.315 \\ 67.577 \\ 1.897 \end{bmatrix} \quad \mathbf{C}_{H/R}^{\rm 2obs} = \begin{bmatrix} 137.15 & 0.244 & 1.396 \\ 0.244 & 28.919 & 0.500 \\ 1.396 & 0.500 & 2.598 \end{bmatrix}$$

$$\mathbf{m}_{H}^{\rm 2obs} = \begin{bmatrix} 0.195 \\ 61.561 \\ -0.092 \end{bmatrix} \quad \mathbf{C}_{H}^{\rm 2obs} = \begin{bmatrix} 130.94 & 1.596 & 0.002 \\ 1.596 & 60.284 & -0.195 \\ 0.002 & -0.195 & 0.101 \end{bmatrix}$$

$$\mathbf{m}_{G/SH}^{\rm 2obs} = \begin{bmatrix} -20.07 \\ 42.937 \\ 0.873 \end{bmatrix} \quad \mathbf{C}_{G/SH}^{\rm 2obs} = \begin{bmatrix} 307.6 & -1.719 & 0.205 \\ -1.719 & 41.057 & 0.342 \\ 0.205 & 0.342 & 0.183 \end{bmatrix}$$

$$\mathbf{m}_{DS}^{\rm 2obs} = \begin{bmatrix} -24.942 \\ 31.659 \end{bmatrix} \quad \mathbf{C}_{DS}^{\rm 2obs} = \begin{bmatrix} 220.34 & -0.025 \\ -0.025 & 65.962 \end{bmatrix}$$

$$\mathbf{m}_{WS}^{\rm 2obs} = \begin{bmatrix} 0.055 \\ 38.103 \\ 1.128 \end{bmatrix} \quad \mathbf{C}_{WS}^{\rm 2obs} = \begin{bmatrix} 2.118 & 0.009 & 0.000 \\ 0.009 & 12.429 & 0.537 \\ 0.000 & 0.537 & 0.029 \end{bmatrix}$$

$$\mathbf{m}_{IC}^{\rm 2obs} = \begin{bmatrix} -38.297 \\ 18.841 \\ 0.492 \end{bmatrix} \quad \mathbf{C}_{IC}^{\rm 2obs} = \begin{bmatrix} 369.25 & -4.503 & 0.089 \\ -4.503 & 66.811 & 0.971 \\ 0.089 & 0.971 & 1.318 \end{bmatrix}.$$

Three-Observable Radar Measurements

In this case, we are supposing to have at disposal a column vector of measurements $\mathbf{x} = [T, Z_{\rm hh}, Z_{\rm dr}, K_{\rm dp}]^{\rm T}$ with T in degree Celsius, $Z_{\rm hh}$ in decibels with respect to the radar reflectivity factor, $Z_{\rm dr}$ in decibels, and $K_{\rm dp}$ in degrees per kilometer

$$\mathbf{m}_{LD}^{\rm 3obs} = \begin{bmatrix} 15.106 \\ 42.946 \\ 4.717 \\ 0.318 \end{bmatrix}$$

$$\mathbf{C}_{LD}^{\rm 3obs} = \begin{bmatrix} 133.86 & 2.276 & 0.245 & -0.144 \\ 2.276 & 61.947 & 4.082 & 2.243 \\ 0.245 & 4.082 & 0.371 & 0.121 \\ -0.144 & 2.243 & 0.121 & 0.119 \end{bmatrix}$$

$$\mathbf{m}_{LR}^{\rm 3obs} = \begin{bmatrix} 20.106 \\ 25.743 \\ 0.548 \end{bmatrix}$$

$$\mathbf{C}_{LR}^{\rm 3obs} = \begin{bmatrix} 133.86 & -2.226 & -0.112 \\ -2.226 & 78.725 & 2.047 \\ -0.112 & 2.047 & 0.071 \end{bmatrix}$$

$$\mathbf{m}_{MR}^{\rm 3obs} = \begin{bmatrix} 20.106 \\ 39.95 \\ 1.375 \\ 0.622 \end{bmatrix}$$

$$\mathbf{C}_{MR}^{\rm 3obs} = \begin{bmatrix} 133.86 & -1.783 & -0.502 & -0.037 \\ -1.783 & 14.216 & 0.887 & 1.556 \\ -0.502 & 0.887 & 0.148 & 0.093 \\ -0.037 & 1.556 & 0.093 & 0.203 \end{bmatrix}$$

$$\mathbf{m}_{HR}^{\rm 3obs} = \begin{bmatrix} 20.106 \\ 54.097 \\ 3.547 \\ 8.090 \end{bmatrix}$$

$$\mathbf{C}_{HR}^{\rm 3obs} = \begin{bmatrix} 133.86 & -0.275 & 2.154 & -0.123 \\ -0.275 & 33.607 & 5.642 & 35.18 \\ 2.154 & 5.642 & 1.257 & 5.026 \\ -0.123 & 35.18 & 5.026 & 47.931 \end{bmatrix}$$

$$\mathbf{m}_{H/R}^{\rm 3obs} = \begin{bmatrix} 10.315 \\ 67.577 \\ 1.897 \\ 10.378 \end{bmatrix}$$

$$\mathbf{C}_{H/R}^{\rm 3obs} = \begin{bmatrix} 137.15 & 0.244 & 1.396 & 2.858 \\ 0.244 & 28.919 & 0.500 & 28.576 \\ 1.396 & 0.500 & 2.598 & 9.892 \\ 2.858 & 28.576 & 9.892 & 93.052 \end{bmatrix}$$

$$\mathbf{m}_{H}^{\rm 3obs} = \begin{bmatrix} 0.195 \\ 61.561 \\ -0.092 \\ -0.160 \end{bmatrix}$$

$$\mathbf{C}_{H}^{\rm 3obs} = \begin{bmatrix} 130.94 & 1.596 & 0.002 & -0.087 \\ 1.596 & 60.284 & -0.195 & -1.639 \\ 0.002 & -0.195 & 0.101 & 0.221 \\ -0.087 & -1.639 & 0.221 & 1.170 \end{bmatrix}$$

$$\mathbf{m}_{G/SH}^{\rm 3obs} = \begin{bmatrix} -20.07 \\ 42.937 \\ 0.873 \\ 0.381 \end{bmatrix}$$

$$\mathbf{C}_{G/SH}^{\rm 3obs} = \begin{bmatrix} 307.6 & -1.719 & 0.205 & 0.806 \\ -1.719 & 41.057 & 0.342 & 2.561 \\ 0.205 & 0.342 & 0.183 & 0.085 \\ 0.806 & 2.561 & 0.085 & 0.303 \end{bmatrix}$$

$$\mathbf{m}_{DS}^{\rm 3obs} = \begin{bmatrix} -24.942 \\ 31.659 \end{bmatrix}$$

$$\mathbf{C}_{DS}^{\rm 3obs} = \begin{bmatrix} 220.34 & -0.025 \\ -0.025 & 65.962 \end{bmatrix}$$

$$\mathbf{m}_{WS}^{\rm 3obs} = \begin{bmatrix} 0.055 \\ 38.103 \\ 1.128 \end{bmatrix}$$

$$\mathbf{C}_{WS}^{\rm 3obs} = \begin{bmatrix} 2.118 & 0.009 & 0.000 \\ 0.009 & 12.429 & 0.537 \\ 0.000 & 0.537 & 0.029 \end{bmatrix}$$

$$\mathbf{m}_{IC}^{\rm 3obs} = \begin{bmatrix} -38.297 \\ 18.841 \\ 0.492 \end{bmatrix}$$

$$\mathbf{C}_{IC}^{\rm 3obs} = \begin{bmatrix} 369.25 & -4.503 & 0.089 \\ -4.503 & 66.811 & 0.971 \\ 0.089 & 0.971 & 1.318 \end{bmatrix}.$$

ACKNOWLEDGMENT

The authors would like to thank Dr. M. Celano and Dr. P. P. Alberoni (ARPA-SIM, Bologna, Italy) for providing radar data and for their helpful suggestions. They would also like to thank the anonymous reviewers for their useful comments.

REFERENCES

[1] M. P. M. Hall, J. W. F. Goddard, and S. M. Cherry, "Identification of hydrometeors and other targets by dual-polarization radar," *Radio Sci.*, vol. 19, pp. 132–140, 1984.

[2] V. N. Bringi, R. M. Rasmussen, and J. Vivekanandan, "Multiparameter radar measurements in Colorado convective storms. Part I: Graupel melting studies," *J. Atmos. Sci.*, vol. 43, no. 22, pp. 2245–2563, Nov. 1986.

[3] K. Aydin, Y. Zhao, and T. A. Seliga, "A differential reflectivity radar hail measurements technique: Observations during the Denver hailstorm of 13 June 1984," *J. Atmos. Ocean. Technol.*, vol. 7, no. 1, pp. 104–113, Feb. 1990.

[4] D. S. Zrnić, V. N. Bringi, N. Balakrishnan, K. Aydin, V. Chandrasekar, and J. Hubbert, "Polarimetric measurements in a severe hailstorm," *Mon. Weather Rev.*, vol. 121, no. 8, pp. 2223–2238, Aug. 1993.

[5] D. S. Zrnić and A. V. Ryzhkov, "Advantages of rain measurements using specific differential phase," *J. Atmos. Ocean. Technol.*, vol. 13, no. 2, pp. 454–464, Apr. 1996.

[6] J. Vivekanandan, D. S. Zrnić, S. M. Ellis, R. Oye, A. V. Ryzhkov, and J. Straka, "Cloud microphysics retrieval using S-band dual-polarization radar measurements," *Bull. Amer. Meteorol. Soc.*, vol. 80, no. 3, pp. 381–388, Mar. 1999.

[7] J. M. Straka, D. S. Zrnić, and A. V. Ryzhkov, "Bulk hydrometeor classification and quantification using polarimetric radar data: Synthesis of relations," *J. Appl. Meteorol.*, vol. 39, no. 8, pp. 1341–1372, Aug. 2000.

[8] D. S. Zrnić, A. V. Ryzhkov, J. Straka, Y. Liu, and J. Vivekanandan, "Testing a procedure for automatic classification of hydrometeor types," *J. Atmos. Ocean. Technol.*, vol. 18, no. 6, pp. 892–913, Jun. 2001.
[9] S. Lim, V. Chandrasekar, and V. N. Bringi, "Hydrometeor classification system using dual-polarization radar measurements: Model improvements and *in situ* verification," *IEEE Trans. Geosci. Remote Sens.*, vol. 43, no. 4, pp. 792–801, Apr. 2005.
[10] P. P. Alberoni, D. S. Zrnić, A. V. Ryzhkov, and L. Guerrieri, "Use of a fuzzy logic classification scheme with a C-band polarimetric radar: First results," in *Proc. ERAD*, 2002, pp. 324–327.
[11] T. D. Keenan, "Hydrometeor classification with a C-band polarimetric radar," *Aust. Meteorol. Mag.*, vol. 52, no. 1, pp. 23–31, 2003.
[12] L. Baldini, E. Gorgucci, and V. Chandrasekar, "Hydrometeor classification methodology for C-band polarimetric radars," in *Proc. ERAD*, 2004, pp. 62–66.
[13] M. Galletti, P. P. Alberoni, V. Levizzani, and M. Celano, "Assessment and tuning of the behaviour of a microphysical characterisation scheme," *Adv. Geosci.*, vol. 2, pp. 145–150, 2005.
[14] L. Baldini, E. Gorgucci, V. Chandrasekar, and W. Peterson, "Implementation of CSU hydrometeor classification scheme for C-band polarimetric radars," in *Proc. 32nd Conf. Radar Meteorol.*, 2005. n. P11R4.
[15] J. W. Conway, D. Nealson, J. J. Stagliano, A. V. Ryzhkov, L. Venkatramani, and D. S. Zrnić, "A new C-band polarimetric radar with simultaneous transmission for hydrometeor classification and rainfall measurement," in *Proc. 32nd Conf. Radar Meteorol.*, 2005. n. P12R14.
[16] A. V. Ryzhkov and D. S. Zrnić, "Radar polarimetry at S, C and X bands, comparative analysis and operational implications," in *Proc. 32nd Conf. Radar Meteorol.*, 2005. n. 9R3.
[17] J. J. Gourley, P. Tabary, and J. Parent du Chatelet, "Classification of hydrometeors and non-hydrometeors using polarimetric C-band radar," in *Proc. 32nd Conf. Radar Meteorol.*, 2005. n. 11R4.
[18] F. S. Marzano, D. Scaranari, M. Celano, P. P. Alberoni, G. Vulpiani, and M. Montopoli, "Hydrometeor classification from dual-polarized weather radar: Extending fuzzy logic from S-band to C-band data," *Adv. Geosci.*, vol. 7, pp. 109–114, 2006.
[19] D. Scaranari, F. S. Marzano, G. Vulpiani, M. Montopoli, M. Celano, and A. Alberoni, "Hydrometeor supervised classification using a bistatic dual-polarized weather radar configuration at C-band," in *Proc. ERAD*, Barcelona, Spain, Sep. 18–23, 2006.
[20] F. S. Marzano, A. Mugnai, G. Panegrossi, N. Pierdicca, E. A. Smith, and J. Turk, "Bayesian estimation of precipitating cloud parameters from combined measurements of spaceborne microwave radiometer and radar," *IEEE Trans. Geosci. Remote Sens.*, vol. 37, no. 1, pp. 596–613, Jan. 1999.
[21] M. Barkat, *Signal Detection and Estimation*. Norwood, MA: Artech House, 1991.
[22] E. Kalnay, *Atmospheric Modeling, Data Assimilation and Predictability*. Cambridge, U.K.: Cambridge Univ. Press, 2002.
[23] V. N. Bringi and V. Chandrasekar, *Polarimetric Doppler Weather Radar*. Boston, MA: Cambridge Univ. Press, 2001.
[24] M. I. Mishchenko and L. D. Travis, "Capabilities and limitations of a current Fortran implementation of the T-matrix method for randomly oriented, rotationally symmetric scatterers," *J. Quant. Spectrosc. Radiat. Transf.*, vol. 60, no. 3, pp. 309–324, 1998.
[25] G. Vulpiani, F. S. Marzano, V. Chandrasekar, and S. Lim, "Constrained iterative technique with embedded neural-network for dual-polarization radar correction of rain path attenuation," *IEEE Trans. Geosci. Remote Sens.*, vol. 43, no. 10, pp. 2305–2314, Oct. 2005.
[26] F. S. Marzano, D. Scaranari, and G. Vulpiani, "Supervised fuzzy-logic classification of hydrometeors using C-band weather radars," *IEEE Trans. Geosci. Remote Sens.*, vol. 45, no. 11, pp. 3784–3799, Nov. 2007.
[27] N. R. Draper and H. Smith, *Applied Regression Analysis*, 2nd ed. New York: Wiley, 1981.
[28] J. M. Bernardo and A. F. M. Smith, *Bayesian Theory*. New York: Wiley, 1994.
[29] J. A. Richards and X. Jia, *Remote Sensing Digital Image Analysis: An Introduction*, 4th ed. Berlin, Germany: Springer-Verlag, 2006.
[30] T. M. Lillesand and R. W. Kiefer, *Remote Sensing and Image Interpretation*, 3rd ed. New York: Wiley, 1994.
[31] J. Testud, E. Le Bouar, E. Obligis, and M. Ali-Mehenni, "The rain profiling algorithm applied to polarimetric weather radar," *J. Atmos. Ocean. Technol.*, vol. 17, no. 3, pp. 332–356, Mar. 2000.
[32] P. L. Heinselman and A. V. Ryzhkov, "Validation of polarimetric hail detection," *Weather Forecast.*, vol. 21, no. 5, pp. 839–850, Oct. 2006.
[33] A. Waldvogel, B. Federer, and P. Grimm, "Criteria for the detection of hail cells," *J. Appl. Meteorol.*, vol. 18, no. 12, pp. 1521–1525, Dec. 1979.
[34] L. Delobbe, I. Holleman, D. Dehenauw, and J. Neméghaire, "Verification of radar-based hail detection product," in *Proc. WWRP Int. Symp. Nowcasting Very Short Range Forecasting (WSN)*, Toulouse, France, 2005. n. 8.1.
[35] A. Witt, M. D. Eilts, G. J. Stumpf, J. T. Johnson, E. D. Mitchell, and K. W. Thomas, "An enhanced hail detection algorithm for the WSR-88D," *Weather Forecast.*, vol. 13, no. 2, pp. 286–303, Jun. 1998.
[36] E. Gorgucci, V. Chandrasekar, V. N. Bringi, and G. Scarchilli, "Estimation of raindrop size distribution parameters from polarimetric radar measurements," *J. Atmos. Ocean. Technol.*, vol. 59, no. 15, pp. 2373–2384, Aug. 2002.
[37] V. N. Bringi, T. Tang, and V. Chandrasekar, "Evaluation of a new polarimetrically based $Z-R$ relation," *J. Atmos. Ocean. Technol.*, vol. 21, no. 4, pp. 612–623, Apr. 2004.

Frank Silvio Marzano (S'89–M'99–SM'03) received the Laurea degree (*cum laude*) in electrical engineering and the Ph.D. degree in applied electromagnetics from the University of Rome "La Sapienza," Rome, Italy, in 1988 and 1993, respectively.

In 1993, he collaborated with the Institute of Atmospheric Physics, National Research Council, Rome. From 1994 to 1996, he was with the Italian Space Agency, Rome, as a Postdoctorate Researcher. After being a Lecturer with the University of Perugia, in 1997, he was with the Department of Electrical Engineering and cofounded the Center of Excellence CETEMPS, University of L'Aquila, L'Aquila, Italy, coordinating the Satellite and Radar Remote Sensing Laboratory. Since 2005, he has been with the Department of Electronic Engineering, University of Rome "La Sapienza," where he is currently teaching courses on antennas, propagation, and remote sensing. His current research concerns passive and active remote sensing of the atmosphere from ground-based, airborne, and spaceborne platforms, with a particular focus on precipitation using microwave and infrared data, development of inversion methods, radiative transfer modeling of scattering media, and radar meteorology issues. He is also involved on radiopropagation topics in relation to incoherent-wave modeling, scintillation prediction, and rain-fading analysis along satellite microwave links.

Dr. Marzano was the recipient of the Young Scientist Award of the XXIV International Union of Radio Science (URSI) General Assembly in 1993. He was the recipient of the ARPAD award from the National Research Laboratory, Washington, DC, in 1998. In 2001, he was the Italian national delegate for the European COST actions n.720 and n.280. Since January 2004, he has been acting as an Associate Editor of IEEE GEOSCIENCE AND REMOTE SENSING LETTERS.

Daniele Scaranari received the Laurea degree (*cum laude*) in electronic engineering and the Master's degree in satellites and orbiting platforms from the University of Rome "La Sapienza," Rome, Italy, in 2005 and 2006, respectively.

He was with the Department of Electronic Engineering, University of Rome "La Sapienza" to cooperate on radar remote sensing of rainfall. He was with the End-to-End Observation Systems Engineering Team, Alcatel Alenia Space, Rome. He is currently with Sofiter System Engineering, Rome, Italy.

Mario Montopoli received the Laurea degree in electronic engineering from the University of L'Aquila, L'Aquila, Italy, in 2004. He is currently working toward the Ph.D. degree in radar meteorology in a joint program between the University of Basilicata, Potenza, Italy, and the University of Rome "La Sapienza," Rome, Italy.

Since 2005, he has been with the Center of Excellence CETEMPS, University of L'Aquila, as a Research Scientist on ground-based radar meteorology, focusing on C-band applications and processing techniques. Since 2006, he has also been a Research Assistant with the Department of Electrical and Information Engineering, University of L'Aquila.

Gianfranco Vulpiani (M'06) received the Laurea degree in physics and the Ph.D. degree in radar meteorology from the University of L'Aquila, L'Aquila, Italy, in 2001 and 2005, respectively.

In 2001, he was with the Department of Physics and the Center of Excellence CETEMPS, University of L'Aquila, as a Research Scientist on ground-based radar meteorology, with special focus on C-band applications and polarimetric applications. He was a Visiting Scientist with Colorado State University, Fort Collins, in 2004. In 2006, he joined the Department of Observation Systems at Météo France in Paris (France) as post-doctoral researcher. Within the framework of the European project FLYSAFE, he has worked on the development of dual-polarization retrieval techniques with a special focus on attenuation correction and hail detection. Since March 2007, he has been employed by the Department of Civil Protection, Rome, Italy, in charge of the managing the Italian Radar Network. He is a Reviewer for several international journals in remote-sensing topics.